Super-resolution Reconstruction of Fetal Brain MRI

Ali Gholipour, Simon K. Warfield

Children's Hospital Boston, Harvard Medical School
300 Longwood Ave. Boston MA 02115 USA
ali.gholipour@childrens.harvard.edu, simon.warfield@childrens.harvard.edu

Abstract. Current fetal MRI practice involves fast 2D slice acquisitions. The reconstruction of volumetric fetal brain MRI from these acquisitions and its post-processing is greatly desired for studying in-utero brain development. The previously developed reconstruction techniques rely on iterations of slice-to-volume registration and scattered data interpolation. In contrast, the technique introduced here is based on a slice acquisition model, and refines the reconstructed volumetric image through a maximum likelihood error minimization approach. Qualitative and quantitative evaluation results show improved sharpness of the reconstructed images using the developed technique. The increased image sharpness measures and lower registration error metrics both indicate more accurate slice motion correction. This in-turn indicates that better volumetric images were reconstructed and used in registration iterations.

1. Introduction

Magnetic resonance imaging (MRI) has become an excellent tool for studying the dynamics of brain maturation, brain development, and the mechanism of brain injury in newborns and preterm infants [1,2]. For these applications, high-resolution volumetric MRI is utilized. Nevertheless 3D MRI of preterm newborns only provides databases for high gestational ages, and moreover it cannot be used for studying normal brain development. This raises great desire for volumetric fetal MRI. But 3D fetal MRI cannot be acquired in-utero mainly because of fetal and maternal motion and the thick slice acquisition necessary for good signal-to-noise-ratio (SNR). The consequent lack of volumetric fetal brain MRI data is a major limitation. However, there have been recent studies reporting quite promising results for the reconstruction of 3D volumetric fetal brain MRI from fast slice acquisitions [3,4].

In order to deal with fetal motion only fast imaging protocols such as 2D single-shot fast spin echo (SSFSE) and echo-planar imaging (EPI) are used in fetal MRI practice [1]. T2-weighted SSFSE is particularly useful in studying brain structure and structural abnormalities as it provides very high in-plane resolution. Motion of the fetus does not frequently affect the in-plane slice quality and resolution of SSFSE, but severe inter-slice artifacts appear in out-of-plane views. The acquisition of useful slices in these cases can be quite laborious as the radiologist need to keep tracking the fetus position and orientation and plan for the desired oblique acquisitions. After all, the images are only good in the slice plane views and no useful 3D image is obtained. State-of-the-art in image processing shows that volumetric images can be obtained by fusing multiple multi-slice scans acquired in orthogonal planes.

Image Analysis for the Developing Brain (MICCAI Workshop)
London, UK, September 24th, 2009

The previous techniques for the reconstruction of high-resolution fetal brain MRI [3,4] are based on iterations of slice-to-volume registration and scattered data interpolation (SDI) and are classified as SDI approaches here. The main technical difference between the two main techniques in this category is that local neighbourhood Gaussian kernel-based scattered data interpolation has been used in [3], while a regular grid of control-points cubic B-Spline scattered data interpolation [5] has been used in [4]. There are also implementation differences between the two techniques for instance in slice-to-volume registration [3,4,6]. But none of these techniques provide an appropriate mathematical formulation for the convergence of the reconstruction to at least a local optimum solution.

The novel technique described here is based on an inner loop of maximum likelihood super-resolution reconstruction which guarantees the convergence of the reconstructed image to match the motion-corrected slices through steepest descent error minimization. The reconstruction is mathematically formulated as an inverse problem of finding the underlying structure which generates the acquired thick-slice MR images. Therefore a 3D slice acquisition model based on subject motion, slice selection and MR signal averaging is established. By using this model the super-resolution reconstruction is formulated as a maximum likelihood minimization of a distance measure between the reconstructed image and the acquired slices. The mathematical formulation and technical details of the method are discussed in section 2. The results reported in section 3 show the improvement achieved by this technique as compared to the scattered data interpolation (SDI) approach. Section 4 contains the concluding remarks.

2. Methodology

2.1. Slice Acquisition Model

A very important approach in super-resolution reconstruction of an imaged object from low-resolution image acquisitions is to formulate an observation model [7]. A good observation model involves different blocks formulating how the acquired images are related to the original scene. For the digital images obtained using camera sensors these blocks include motion effects, atmospheric and sensor blur effects (modelled with point spread functions), and down-sampling [7].

There are differences between the observation model of digital camera imaging and the image acquisition model of MRI. The most important difference is that the digital camera observation models are often two-dimensional. In MRI, 3D reconstruction is desired and the thickness of the acquired slices and their physical coordinates and orientation must be considered in 3D space. Particularly in fetal MRI, slice acquisitions are performed interactively with varying parameters according to fetus position and motion during the time of acquisition. Slice spacing is normally 4 to 6 times larger than the matrix spacing causing severe partial voluming. Therefore an appropriate model of slice selection and signal averaging is needed. Similarly, full 6-DOF 3D rigid motion is observed in fetal MRI while it is often limited to 2D shift and rotation in super-resolution reconstruction. Finally the number of slice acquisitions is limited by the time allowed for fetal MRI and the slice quality highly varies depending on the motion, noise, and magnetic field inhomogeneity. The slice quality strongly affects the quality of reconstruction.

In a trade-off between a realistic model and a feasible solution, the following slice acquisition model is considered in this study:

$$\underline{Y}_k = \mathbf{D}_k\mathbf{B}_k\mathbf{S}_k\mathbf{M}_k\underline{X} + \underline{V}_k \quad , \quad k = 1,...,n \tag{1}$$

where $\underline{Y}_k$ is the vector of the voxels of the k^{th} 2D slice with slice thickness Δs_k and uniform in-plane spacing of L_k; $\underline{X}$ is a vector of the desired uniformly-sampled reconstructed image voxels in the lexicographical order with uniform spacing of $\Delta\rho$; $\underline{V}_k$ is a Gaussian noise vector, n is the number of slices obtained from N scans, $\mathbf{M}_k$ is the matrix of motion parameters, $\mathbf{S}_k$ is a matrix representing the slice selection profile, $\mathbf{B}_k$ is a blur matrix representing the point spread function of the MRI signal acquisition process, and $\mathbf{D}_k$ is a down-sampling matrix.

The slice selection profile, generated by a truncated Sinc pulse envelope function, is a boxcar function multiplied by a linear phase shift in the slice select direction. The linear phase shift is compensated by applying a refocusing gradient in a procedure called post-excitation rephasing [8]. Assuming negligible pulse truncation effects and cross-talk artifacts, the slice selection profile can be modeled by a box car function. Consequently the slice selection profile is geometrically described by

$$\left|\vec{\mu}_{sk}.\vec{r} - s_{0k}\right| < \Delta s_k/2 \tag{2}$$

where Δs_k is the slice thickness, s_{0k} is the distance of the slice from the origin, and $\vec{\mu}_{sk}$ specifies the slice (or slice-selection) orientation. $\vec{\mu}_{sk}$ is interpreted as the normal vector of the slice plane equation. This model can be interpreted as region selection, signal averaging and resampling in the image space. The implementation details of generating $\mathbf{S}_k$ from this model will be discussed in section 2.3.

2.2. Super-resolution Reconstruction

The maximum likelihood (ML) estimation of the super-resolution problem defined by equation (1) can be written as the maximization of the likelihood probability density function (PDF) of the acquired slices given the reconstructed image, i.e. $\Pr(\underline{Y}_k \mid \underline{X})$. Assuming an exponential model for PDFs based on a distance d between the model and the acquired slices $\underline{Y}_k$, the maximization of the log-likelihood function results in:

$$\underline{\hat{X}} = \underset{\underline{X}}{ArgMin}\left[\sum_{k=1}^{N} d\left(\underline{Y}_k, \mathbf{D}_k\mathbf{B}_k\mathbf{S}_k\mathbf{M}_k\underline{X}\right)\right] \tag{3}$$

When the noise is Gaussian, the least squares solution of (3) results in ML estimation. The least squares solution minimizes the L_2 norm of the error:

$$\underline{\hat{X}} = \underset{\underline{X}}{ArgMin}\left[\sum_{k=1}^{N} \left\|\mathbf{D}_k\mathbf{B}_k\mathbf{S}_k\mathbf{M}_k\underline{X} - \underline{Y}_k\right\|_2^2\right] \tag{4}$$

When the number of acquired slices is small the problem will be underdetermined. In this case regularization terms can be added to the cost function to enforce a

constrained minimal norm solution. An appropriate regularization term penalizes the high-energy components in the estimated image, thus it can be formulated by the L_2 norm of a high-pass filtered image. The modified minimization problem is written as

$$\underline{\hat{X}} = \underset{\underline{X}}{ArgMin}\left[\sum_{k=1}^{N}\left\|\mathbf{D}_k\mathbf{B}_k\mathbf{S}_k\mathbf{M}_k\underline{X}-\underline{Y}_k\right\|_2^2+\lambda\left\|\mathbf{C}\underline{X}\right\|_2^2\right] \quad (\mathbf{5})$$

Where **C** is a positive definite matrix and λ is the Lagrange multiplier.

2.3. Implementation

The steepest descent iterative solution of the minimization in (5) is written as:

$$\underline{\hat{X}}^{n+1} = \underline{\hat{X}}^{n} + \alpha\left[\sum_{k=1}^{N}\mathbf{M}_k^{\mathrm{T}}\mathbf{S}_k^{\mathrm{T}}\mathbf{B}_k^{\mathrm{T}}\mathbf{D}_k^{\mathrm{T}}\left(\underline{Y}_k-\mathbf{D}_k\mathbf{B}_k\mathbf{S}_k\mathbf{M}_k\underline{\hat{X}}^{n}\right)-\lambda\mathbf{C}^{\mathrm{T}}\mathbf{C}\underline{\hat{X}}^{n}\right] \quad (\mathbf{6})$$

where α is the step size in the direction of the gradient.

The matrices **C, D**$_k$, **B**$_k$, **S**$_k$, and **M**$_k$ and their transposes are exactly interpreted as corresponding image operators. **C** is the gradient magnitude image operation. For simplicity the desired reconstructed image spacing is considered to be equal to the in-plane spacing (matrix resolution), hence L_k=1 and $\mathbf{D}_k$=**I**. **B**$_k$ is defined as the convolution with a Gaussian kernel resembling the point spread function (PSF) of the MRI signal acquisition process. **S**$_k$ is defined for each slice based on equation (2); the slice plane normal vector $\vec{\mu}_{sk}$ and the distance s_{0k} are computed based on the direction cosines matrix and the origin of each slice, respectively. This operation is implemented as rigid 3D rotation with the rotation matrix directly obtained from direction cosines matrix, and its transpose is the inverse (transpose) of the direction cosines matrix. The motion matrix **M**$_k$ is implemented as a 6-DOF 3D rigid transformation and is defined for each slice through slice-to-volume registration, which will be discussed later in this section. The image operations are applied to the reconstructed image and their transposes are applied to the error image exactly as suggested by equation (6). On the basis of the nominal values of error and the gradient magnitude images, $\alpha = 0.5$ and $\lambda = 0.1$ were used in the experiments.

Figure 1 shows the block diagram of the inner and outer loops of the entire volume reconstruction algorithm. The inner loop involves the maximum likelihood super-resolution reconstruction based on equation (6). The outer loop involves slice-to-volume registration and scattered data interpolation. X_R is the reference volume for registration, which is initially obtained by averaging the acquired thick slice scans, and is set to be the reconstructed image after the initial estimation. During the iterations the reconstructed image which is used as the reference volume for registration improves and hence more accurate slice-to-volume registration (slice motion correction) is achieved. The termination condition of the inner loop (tc1) is satisfied when the normalized cost function in equation (5) or its deviation go below a threshold. This threshold is set to be 1e-5 for the norm of the cost function over the norm of the reconstructed image in our experiments. The termination condition for the outer loop (tc2) is satisfied when the decrease in the root mean square error of the slice-to-volume registration metrics goes below a threshold in two consecutive iterations. The best reconstructed image is then considered as the output.

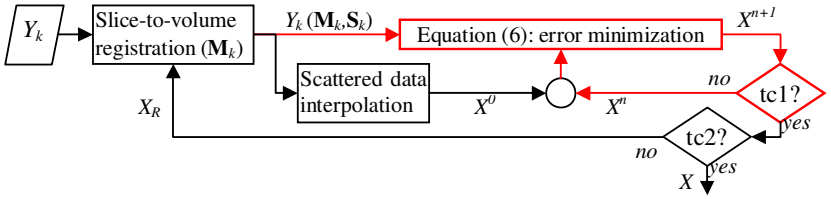

Fig. 1. Block diagram of the inner (red) and outer loops of the developed super-resolution reconstruction algorithm; tc1 and tc2 represent the termination conditions of the inner and the outer loops respectively. Note that the SDI approach only involves the outer loop. In this case the output of scattered data interpolation block directly goes to tc2.

The two remaining blocks include slice-to-volume registration and scattered data interpolation. A robust algorithm has been developed for slice-to-volume registration. This algorithm works in three stages. In each stage, a 6-DOF rigid transformation is computed for a subset of slices. In the first stage, the subset involves slices acquired in one stack of the interleaved acquisition; for example, in a dual interleaved acquisition, two subsets are used: subset of even slices and subset of odd slices. In the second stage of registration, the rigid transformation of each slice is refined based on a subset including the slice and its two interleaved neighbors. For example, in a dual interleaved acquisition the transformation of slice 5 is computed based on registering the set of slices 3, 5, and 7 to the reference volume. Finally, in the third stage, only the source slice is used for registration. The algorithm minimizes the mean square intensity differences between each subset of slices and the reference volume. Powel optimization with step sizes of 0.05, 0.02, and 0.02 was used in the three stages of registration, respectively.

The scattered data interpolation method implemented here outperformed the previous methods [3,4] in our experiments. It is an efficient weighted local intensity injection approach based on cubic B-Spline kernels: In order to account for the slice thickness the motion corrected slices are first resampled in the slice select direction using nearest neighbour interpolation. The scattered data points obtained from motion-corrected resampled slices are then mapped to the nearest neighbour grid points in the reconstructed image space and their intensity values are injected into the neighbourhood points using cubic B-Spline kernel. In the experimental results that follow, the developed technique (referred to as MLE) is compared to the SDI approach which only involves the outer loop of the algorithm illustrated above.

3. Results

3.1. Data Acquisition and Visual Assessment of the Reconstruction Quality

Data was obtained from clinical MRI of patients with diagnosed or suspected cases of fetal anomalies after diagnostic ultrasonography. Clinical fetal MRI was performed using a 1.5-T TwinSpeed Signa system (GE healthcare) and an 8-channel phased-array cardiac coil, without maternal sedation or breath-hold, with the mother in left

decubitus position to minimize caval compression. The protocol involved acquisitions in the fetal sagittal, axial and coronal views using half-Fourier acquisition single-shot fast spin echo (SSFSE) magnetic resonance imaging with TR varying between 1000 and 4500; TE varying between 80 and 100; number of excitations 0.5; variable field of view based on the maternal and fetal body size (between 24-40 cm); variable matrix size between 160 and 512; and slice thickness of 3 or 4 mm.

High-quality slices are normally obtained, however, due to the fetal and maternal motion there are normally considerable out-of-plane artifacts. But occasionally motion-induced intensity distortions and signal loss artifacts corrupt a few slices. Ten datasets were used in this study, which were obtained for fetuses in the GA range of 19.28 to 35.43 weeks (mean 26.33, STD 6.34). A subset of acquired scans in each dataset was pre-selected based on visual inspection. The number of input scans used in reconstruction (N) was between 3 and 11 (mean 6.1, STD 2.5). Low-quality and motion-corrupted slices with low SNR (SNR lower than two standard deviations from the average slice SNRs) were automatically omitted from the reconstruction process.

Figure 2 shows the reconstruction of images for the first dataset (GA 19.28, N= 5). The rows show slices of three orthogonal views, i.e. axial, coronal, and sagittal. The first three columns show three original SSFSE scans acquired in the axial, coronal, and sagittal planes. Figure 2(d) shows the reconstruction by the SDI approach and (e) shows the reconstruction by the developed MLE approach.

Fig. 2. Slices of the first dataset: axial, coronal, and sagittal views of the acquired (a) axial, (b) coronal, (c) sagittal SSFSE scans; the reconstructed images using (d) the SDI approach, and (e) the developed MLE approach. (a)-(c) are only good in slice plane view. The volumetric image in (e) is good in all views and is more accurate and sharper than (d).

The visual inspection evaluation results show that good-quality uniformly-sampled volumetric reconstructed images were obtained for 9 datasets. Mis-registration artifacts were observed in the reconstructed images for the 10th dataset (GA 35.43, *N*=6) using both techniques, and for the 2nd dataset (GA 19.28, *N*=5) using the SDI technique only. In all cases the images obtained by the developed MLE technique had higher contrast and sharper edges and structures than the images obtained by SDI. These observations are supported by the quantitative evaluation in the next section.

3.2. Quantitative Evaluation Results

Two sets of metrics have been used to evaluate and compare the effectiveness of the developed MLE technique as compared to the SDI approach. The first metric is the root mean square error (RMSE) of intensity values of the motion-corrected slices and the reference reconstructed images. Figure 3 compares the final average registration metrics obtained for the ten datasets using the SDI and MLE techniques as compared to the registration metric in the first iteration. Since the average of input scans was used as the initial registration target image, the first iteration metrics are shown by AVE in the chart. Obviously lower registration metrics indicate better reconstructed target images. It is observed that except in one case (dataset 7), in all other cases improvement was achieved by using the MLE technique. The motion was negligible for the 7th dataset (GA 31.43, *N*=6) and the output was generated in the first iteration.

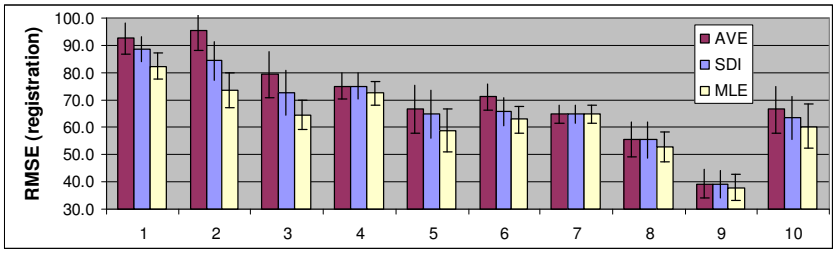

Fig. 3. The comparison of the RMSE of intensity values (registration metrics) between slices and the reference reconstructed images for ten fetal brain MRI datasets; (AVE): initial registration metric using the average image as the target registration volume, (SDI): minimum metric using the SDI approach, and (MLE): minimum metric using the developed MLE technique. Except in one case (dataset 7) in which the motion was negligible, in all other cases the metric was lower for the MLE technique as compared to both AVE and SDI techniques.

The second set of metrics is from the class of sharpness (focus) measures. The rational behind using sharpness measures is that when there are uncorrected motion or error residuals between the input image acquisitions, the average image will be an out-of-focus motion blurred version of the imaged structure. When the motion is more effectively estimated and corrected and the motion-corrected images are more accurately fused in the reconstruction process, sharper structures appear in the reconstructed image. Two sharpness measures are used in this study: $M1$ (the intensity variance measure) and $M2$ (the energy of image gradient measure). Both measures are monotonic and robust to noise [9]. The variance measure is calculated as the sum of

square differences (SSD) between each voxel intensity value and the mean image intensity value. $M2$ is computed by integrating the magnitude of image gradient at all voxels. Table 1 shows the summary of the statistics of these two measures. The first three columns show the average of the measures over ten datasets. It is observed that both measures show improved sharpness by MLE technique. The next three columns show the percentage of datasets for which the measures satisfied the tested comparison conditions. On the basis of these results MLE provides higher sharpness measures for all datasets as compared to both average and SDI techniques.

Table 1. Statistics and comparison of the sharpness measures for MLE, SDI and AVE.

	mean(AVE)	mean(SDI)	mean(MLE)	SDI > AVE	MLE > AVE	MLE > SDI
$M1$	4.06E+04	4.14E+04	4.38E+04	80% (8/10)	100% (10/10)	100%
$M2$	1.67E+10	1.62E+10	1.92E+10	40% (4/10)	100% (10/10)	100%

4. Conclusion

An iterative steepest descent error minimization approach has been utilized as the solution of the ML formulation of the fetal brain MRI super-resolution reconstruction. This formulation is obtained from a slice acquisition model which takes into account models of motion, slice selection, signal blur, and sampling of the fast MRI slice acquisition. The obtained results, in specific the comparison of average registration error metrics and two sharpness measures show that the developed technique provides improvements over the conventional scattered data interpolation approach.

Acknowledgements

This research was supported in part by NIH grants R01 RR021885, R01 GM074068 and R01 EB008015.

References

1. Prayer D, Brugger PC, Prayer L. Fetal MRI: techniques and protocols, Pediatr Radiol 2004; 34:685-693.
2. Rutherford M, Jiang S, Allsop J, Perkins L, Srinivasan L, Hayat T, Kumar S, Hajnal J. MR imaging methods for assessing fetal brain development. Dev Neurobiol. 2008; 68:700-11.
3. Rousseau F, Glenn OA, Iordanova B, Rodriguez-Carranza C, Vigneron DB, Barkovich JA, Studholme C. Registration-based approach for reconstruction of high-resolution in utero fetal MR brain images. Acad Radiol. 2006 Sep; 13(9):1072-81.
4. Jiang S, Xue H, Glover A, Rutherford M, Rueckert D, Hajnal JV. MRI of moving subjects using multislice snapshot images with volume reconstruction (SVR): application to fetal, neonatal, and adult brain studies. IEEE Trans Med Imaging. 2007 Jul; 26(7):967-80.
5. Lee S, Wolberg G, Shin SY. Scattered data interpolation with multilevel B-Splines. IEEE Trans Visual Comp Graph. 1997; 3(3):228-244.
6. Kim K, Hansen M, Habas P, Rousseau F, Glenn O, Barkovich AJ, Studholme C. Intersection based registration of slice stacks to form 3D images of the human fetal brain. Proc 5th IEEE Int Sym Biomed Imag: From Nano to Macro. 2008 May; 1167-1170.
7. Park SC, Park MK, Kang MG. Super-resolution image reconstruction: a technical overview. IEEE Signal Processing Magazine. 2003;20(3):21-36.
8. Liang ZP, Lauterbur PC. Principles of Magnetic Resonance Imaging. 2000; IEEE Press.
9. Subbarao M, Choi T, Nikzad A. Focusing techniques. Optical Engineering. 1993;32(11):2824-2836.